Revised manuscript: MOLCAA-D-18-00847

Octyl and propylsulfonic acid co-fixed Fe_3O_4@SiO_2 as a magnetically separable, highly active and reusable solid acid catalyst in water

Nuryono Nuryono[1]*, Ani Qomariyah[1], Wontae Kim[2], Ryoichi Otomo[3], Bambang Rusdiarso[1], Yuichi Kamiya[3]*

[1]Department of Chemistry, Universitas Gadjah Mada, Yogyakarta 55281, Indonesia

[2]Graduate School of Environmental Science, Hokkaido University, Japan

[3]Faculty of Environmental Earth Science, Hokkaido University, Japan

*Corresponding author:

nuryono_mipa@ugm.ac.id (Nuryono Nuryono)

kamiya@ees.hokudai.ac.jp (Yuichi Kamiya)

Abstract

Modifications of propylsulfonic acid-fixed Fe_3O_4@SiO_2 with three organosilanes (C_2, C_8, and phenyl) were investigated to develop a magnetically separable solid acid catalyst active for hydrolysis of ethyl acetate in excess water. Among the organosilanes, triethoxy(octyl)silane was the best modifier for improvement in catalytic activity, with activity of approximately twice that of the unmodified catalyst. The catalytic activity was comparable to those of $Cs_{2.5}H_{0.5}PW_{12}O_{40}$ and $H_3PW_{12}O_{40}$ anchored on hydrophobic SBA-15 if compared per acid sites, though the acid strength of sulfonic acid was much weaker than that of $H_3PW_{12}O_{40}$. High hydrophobicity over the surface and around the acid sites created by the octyl group was responsible for the high catalytic activity and the high stability in water achieved. In addition to the improvement in catalytic activity, modification with the octyl group provided high stability for repeated uses of the catalyst in the reaction and there was little decrease in activity over at least four reuses. The catalyst was easily separated from the reaction solution by application of an external magnetic field.

Keywords: magnetite, silica coating, solid acid, hydrophobicity, ethyl acetate hydrolysis

1. Introduction

There is a growing need for more environmentally benign processes in the chemical industry. This ‘green chemistry’ aims to design chemical products and processes to reduce or eliminate the use or generation of hazardous substances [1]. Catalysis is a key to implementing the principles of green chemistry, because reactions proceed more efficiently and selectively under mild reaction conditions in the presence of catalysts, thereby suppressing the formation of by-products, eliminating waste compounds, and saving energy and additional raw materials [2].

Within catalysis employed for the chemical industry, acid-catalyzed reactions are among the most important [3]. Traditionally and currently, large amounts of liquid acids such as H_2SO_4, HF, $AlCl_3$, and BF_3 are used for the production of various chemicals. However, because of various benefits, including low corrosion activity, safety issues, less waste generation, and easy separation and recovery, these should be replaced by solid acids [4]. However, for reactions in which water participates as a reactant or product, such as hydration, hydrolysis, and esterification, only a few solid acids show acceptable performance [5] and so very large quantities of conventional liquid acids are still utilized

in a number of industrial processes. For replacement of liquid acids, solid acids delivering high levels of activity as well as stability in water should be developed alongside in-depth understanding of catalysis in water.

Sulfonic acid-fixed silica gel, which the pioneering work by Badley and Ford reported in 1989 [6], is a kind of organic-inorganic hybrid material which acts as a solid acid. After the discovery of mesoporous silica, including MCM-41 [7] and FSM-16 [8], research into sulfonic acid-fixed solid acids was expanded into their utilization to improve catalytic activity, especially for acid-catalyzed reactions involving bulky reactants without any mass transfer limitation [9–15]. Apart from the utilization of mesoporous silica, intensive investigations have been carried out into the immobilization of well-designed sulfonic acid precursors on siliceous supports [12, 16–19]. Davis et al. have set out ways of immobilizing well-designed sulfonic acid precursors including disulfide and sulfonate ester on SBA-15 and transforming them into sulfonic acid, to offer control of the spatial arrangement of acid centers and found a cooperative effect between two adjacent sulfonic acids for bisphenol A synthesis [12].

Recently, control of the microenvironment around the active center by organic

modification has been investigated for solid acid catalysts, in which acid components including sulfonic acid [20–24] and Keggin-type heteropolyacid [25] are fixed onto siliceous materials. Thus far, catalysis by solid acid catalysts has been understood basically in terms of three fundamental properties, including types of acid site, acid strength, and acid amount [26]. The control of the microenvironment would be considered another property important for the design of and developments in solid acid catalysts. Yang et al. [20] synthesized propylsulfonic acid functionalized-silica particles with different hydrophobicity by a co-condensation method, with organosilanes having different alkyl chain lengths (C_3, C_8, and C_{16}). They found that a catalyst with a highly hydrophobic surface with a hexadecyl group gave high selectivity for 5-hydroxymethylfurfural (5-HMF) in the dehydration of fructose, due to suppression of the successive rehydration of 5-HMF owing to rapid separation of produced water from the active site. A similar positive effect was also observed in the dehydration of sorbitol to isosorbide catalyzed by propylsulfonic acid-fixed SBA15, by tuning hydrophobicity with different loadings of methyl groups [21]. Wilson and coworkers demonstrated that the acid strength of sulfonic acid in a propylsulfonic group fixed over MCM-41 was restored

to inherent strength by further modification of the octyl group to hinder the interaction of sulfonic acid with silanol on the silica wall [22]. They further demonstrated that octyl and propylsulfonic acid co-grafted SBA-15 was highly tolerant of water for esterification of methanol with acetic acid [23]. Inumaru et al. synthesized an organic-inorganic hybrid heteropolyacid catalyst, in which $H_3PW_{12}O_{40}$ was firmly anchored on the silica wall of SBA-15 by acid-base interaction with a 3-aminopropyl group pre-fixed on the wall and surrounded by octyl groups [25]. This hybrid heteropolyacid catalyst showed excellent catalytic activity for acid sites which was higher than Nafion-H and $Cs_{2.5}H_{0.5}PW_{12}O_{40}$ for hydrolysis of ethyl acetate in water.

Easy and rapid separation of catalysts is essential, especially for practical applications. Magnetic separation is one of the most convenient and efficient techniques for recovery of powdery materials dispersing in liquid phase. Iron oxides are easily available magnetic substances which play a major role in many areas of chemistry, physics, and materials sciences [27]. However, unmodified magnetite nanoparticles tend to aggregate because of their high specific surface area and strong inter-particle interaction. To prevent this aggregation, magnetite nanoparticles are often covered with a

silica shell. Another merit of the silica covering is in providing reaction sites for further modification with organosilanes through covalent Si-O-Si bonds.

In the present study, we investigated modification of propylsulfonic acid-fixed Fe_3O_4@SiO_2 with organosilanes to develop a magnetically separable solid acid catalyst which was highly active and reusable for acid-catalyzed reactions in excess water. To systematically control the hydrophobicity, triethoxy(ethyl)silane and triethoxy(octyl)silane were used for the modification. In addition, to compare aliphatic and aromatic organic groups, triethoxy(phenyl)silane was applied. As a result of comparison, we found that the modification of triethoxy(octyl)silane significantly improved the catalytic activity and stability for hydrolysis of ethyl acetate in water. The reason why we chose to investigate the reaction in excess water was to clearly demonstrate the advantage of the control of the microenvironment around the acid site in such harsh reaction conditions for solid acid catalysts. In addition, hydrolysis of carboxylic acid esters is one of the most important reactions both scientifically and industrially and thus the development of solid acid catalysts with high activity is still keenly desired. To the best of our knowledge, this is the first report to demonstrate the

high catalytic performance of organic and propyl sulfonic acid co-modified solid acid in excess water.

2. Experimental

2.1. Materials synthesis

Series of the prepared samples are illustrated in Scheme 1. Firstly, silica-coated magnetite (Fe_3O_4@SiO_2) was prepared and 3-mercaptopropyl group was fixed on it with different densities. Then, thiol group was oxidized with nitric acid to transform it into sulfuric acid. Finally, the materials were further modified with organosilanes with different organic groups. The preparation procedures are described in detail in the following sections.

2.1.1. Fe_3O_4@SiO_2

Magnetite (Fe_3O_4) was prepared according to a method reported in [27]. Milli-Q water was deaerated by flowing through N_2 for 30 min before use. Two grams of $FeCl_2 \cdot 4H_2O$ (2 mmol, Wako Pure Chem. Ind.), 5.2 g of $FeCl_3 \cdot 6H_2O$ (4 mmol, Wako Pure

Chem. Ind.) and 1 mL of hydrochloric acid (0.1 mol L^{-1}, Wako Pure Chem. Ind.) were added to Milli-Q water (200 mL) and the suspension was stirred at room temperature until the solids were completely dissolved. To the resulting solution, 4 mL of aqueous ammonia (25%, Wako Pure Chem. Ind.) was added. The solution was stirred at room temperature for 3 h and a black suspension was formed. After addition of 100 mL of 2-propanol (Wako Pure Chem. Ind.), the suspension was heated at 40 ºC and then 60 mmol of tetraethoxysilane (TEOS) was added with stirring. The suspension was stirred at room temperature for another 21 h. Throughout all operations, N_2 was passed through the solution. Finally, the suspension was evaporated at 60 ºC. The resulting brown powder was calcined at 250 ºC for 2 h. The obtained solid is denoted as Fe_3O_4@SiO_2. Bare Fe_3O_4 without TEOS addition was also prepared for comparison.

2.1.2 Modification of Fe_3O_4@SiO_2 with 3-mercaptopropyltrimethoxysilane

Fe_3O_4@SiO_2 was dried at 150 °C for 6 h before use. Two grams of Fe_3O_4@SiO_2 and 0.12 g of 3-mercaptotriethoxyproplsilane (MPTES, Wako Pure Chem. Ind.) were added to 9.215 g of toluene (Wako Pure Chem. Ind.). The suspension was refluxed at

120 °C for 4 h with vigorous stirring. After being separated by filtration, the solid was washed with toluene and methanol (about 300 mL of each) and dried at 60 °C for 12 h The obtained solid is denoted as HS(1.1)/Fe_3O_4@SiO_2, in which the figure in parenthesis is the surface density of SH (nm^{-1}) estimated from surface area and elemental analysis.

To investigate the influence of MPTEP loading, samples prepared with different MPTEP doses ranging from 0.02 g (0.03 mmol $g^{-1}_{\_Fe3O4@SiO2}$) to 1.19 g (3.00 mmol $g^{-1}_{\_Fe3O4@SiO2}$) were prepared in a similar manner to HS(1.1)/Fe_3O_4@SiO_2.

2.1.3. Oxidation of HS/Fe_3O_4@SiO_2

Oxidation of the thiol group for HS(1.1)/Fe_3O_4@SiO_2 was carried out with 20% HNO_3 (Wako Pure Chem. Ind.) according to the method reported by Yang et al. [28]. First, 0.5 g of HS(1.1)/Fe_3O_4@SiO_2 was wetted with a small amount of 20 wt% HNO_3. Then, 10 g of 20% HNO_3 was poured over it very slowly. The mixture was then stirred at room temperature for 24 h, and 10 mL Milli-Q water was then added. The obtained powder was separated by filtration, thoroughly washed with Milli-Q water and dried overnight at 60 °C. The resulting sample is denoted as HSO_3(1.1)/Fe_3O_4@SiO_2. For the samples with

different SH densities, the oxidation of SH was conducted using the same procedure as for $HSO_3(1.1)/Fe_3O_4@SiO_2$.

2.1.4. Modification of $HSO_3(1.1)/Fe_3O_4@SiO_2$ with organosilanes

Triethoxy(octyl)silane (0.6 mmol, Wako Pure Chem. Ind.) was added to the suspension of $HSO_3(1.1)/Fe_3O_4@SiO_2$ (1.0 g) in toluene (9.215 g), and the suspension was refluxed at 120 °C for 24 h. After being separated by filtration, the solid was washed with toluene and methanol (about 200 mL of each) and dried at 60 °C for 12 h. The resulting solid is denoted as $Oc/HSO_3(1.1)/Fe_3O_4@SiO_2$. Modifications with triethoxy(ethyl)silane (Wako Pure Chem. Ind.) and triethoxy(phenyl)silane (Wako Pure Chem. Ind.) were also conducted in the same manner as for $Oc/HSO_3(1.1)/Fe_3O_4@SiO_2$, and the obtained materials are denoted as $Ph/HSO_3(1.1)/ Fe_3O_4@SiO_2$ and $Et/HSO_3(1.1)/ Fe_3O_4@SiO_2$, respectively.

2.2. Characterization

Powder X-ray diffraction (XRD) was performed using an X-ray diffractometer

(Rigaku Mini Flex) with Cu Kα radiation (λ = 0.154 nm). Specific surface area was estimated by the Brunauer–Emmett–Teller (BET) equation applied to an adsorption isotherm of N_2 at 77 K, which was acquired on a Belsorp mini instrument (BEL Japan Inc.). The sample was pretreated under N_2 flow at 150 °C for 2 h before measurement. X-ray photoelectron spectra (XPS) were taken on an XPS-7000 instrument (Rigaku) with Mg Kα radiation. Binding energy was calibrated with respect to C 1s at 284.6 eV. Scanning electron microscopy (SEM) images were obtained on an FE-SEM (Hitachi, S-4800). Infrared (IR) spectra of the samples were recorded for self-supporting disks on an IR spectrometer (FT-IR/230, JASCO) at 120 °C in a flow of N_2. Before measurement, the disks were pretreated at 120 °C in a flow of N_2 and the spectra were taken in the flow of N_2 to prevent interference due to adsorbed water.

The amounts of H, C, and S in the samples were determined by the Center for Instrumental Analysis at Hokkaido University (Sapporo, Japan). Silicon to iron ratio (Si/Fe) in the sample was estimated by using an inductively coupled plasma-atomic emission spectrometer (ICP-AES, Shimadzu ICPS-7000). To obtain the solution for the ICP-AES measurement, the sample was dissolved in an aqueous solution of KOH (Wako

Pure Chem. Ind.). Adsorption isotherm of water vapor was obtained at 25 °C on an automatic apparatus (Belsorp 18, BEL Japan Inc.) after the sample was pretreated at 150 °C in a vacuum for 3 h.

Acid amounts in the samples were estimated by a titration method as follows. The sample powder (0.02 g) was added to an aqueous solution of NaCl (1.0 mmol/L, 5 mL, and Wako Pure Chem. Ind.) and the suspension was stirred at room temperature. During the treatment, H^+ in the sample was exchanged with Na^+ in the solution. Only for Oc/HSO_3(1.1)/Fe_3O_4@SiO_2, a small amount of ethanol was added to the solution to get the sample to well disperse in the solution. After 1 h, the suspension was centrifuged to separate the sample powder. Concentration of Na^+ in the solution was determined by using an ion chromatograph (Tosoh Co., IC-2001). A column containing a cation-exchange resin (TSK gel IC-Cation 1/2 HR, Tosoh) and an aqueous solution of methanesulfonic acid (2.2 mmol L^{-1}) and 18-crown-6 (1.0 mmol L^{-1}) was used as stationary and mobile phases, respectively.

2.3. Catalytic hydrolysis of ethyl acetate in water

Hydrolysis of ethyl acetate in excess water was performed in a batch reactor. The catalyst powder (0.1 g), aqueous solution of ethyl acetate (5 wt%, 10 mL), and dihexyl ether (0.18 g, internal standard) were put in the reactor and heated at 60 °C with vigorous stirring. A small portion of the reaction solution was periodically withdrawn, and the catalyst powder was immediately separated by centrifugation. The obtained supernatant was analyzed using a gas chromatograph (Shimadzu, GC-8A) equipped with a Porapak® QS column and a flame ionization detector.

Reusability testing was performed as follows. After 4 h of the reaction, the catalyst was recovered magnetically by putting a magnet on the outer wall of the reactor and the reaction solution was decantated. Then fresh reaction solution was poured and heated at 60 °C to start the reaction (first reuse). This operation was repeated up to fourth reuse.

3. Results and discussion

3.1 Fe_3O_4 and Fe_3O_4@SiO_2

Fig. 1 shows XRD patterns of bare Fe_3O_4, Fe_3O_4@SiO_2, HS(1.1)/Fe_3O_4@SiO_2 and HSO_3(1.1)/Fe_3O_4@SiO_2. Bare Fe_3O_4 gave diffraction lines at 2θ = 30.26, 35.68, 43.44,

and 53.98° (Fig. 1a), which were assigned to (220), (311), (400), and (422) of magnetite (Fe_3O_4), respectively. By using the Scherrer's equation with the diffraction line of (311), the crystallite size of Fe_3O_4 was estimated to be 16.8 nm (D_{XRD}, Table 1). Morphology of bare Fe_3O_4 was observed on an SEM image (Fig. 2a). Bare Fe_3O_4 was composed of spherically shaped particles. One hundred and fifty particles were randomly selected on the SEM images and the size of each particle was measured. The particle sizes were distributed from approximately 8 to 17 nm, with an average diameter of 12.5 nm (D_{SEM}) which was almost the same as the crystallite size estimated by XRD (D_{XRD}).

After coating of Fe_3O_4 with SiO_2, a broad diffraction line due to amorphous SiO_2 appeared at $2\theta = 22°$. The XRD pattern of Fe_3O_4 remained intact though the intensities were decreased (Fig. 1b). The diffraction angles, relative intensities, and crystallite size of the Fe_3O_4 core were not changed by the SiO_2 coating. Since the peak caused by Fe 2p completely disappeared on the XPS spectrum and an intense peak at B.E. = 106.0 eV due to Si 2p emerged for Fe_3O_4@SiO_2 (Fig. 3b), the Fe_3O_4 core was evidently fully covered with the SiO_2 shell. From the size of the Fe_3O_4 core (D_{XRD} = 16.4 nm, Table 1) and the average diameter of the particles (D_{SEM} = 23.0 nm), the thickness of the SiO_2 shell for

Fe_3O_4@SiO_2 was estimated to be about 3.5 nm (Scheme 1).

3.2. *Modification of Fe_3O_4@SiO_2 with MPTES and oxidation of the thiol group into sulfonic acid*

Modification of Fe_3O_4@SiO_2 with MPTES did not change the size and crystalline structure of the Fe_3O_4 core (Fig. 1(c); Table 1). From the elemental analysis, contents of C and S were found to be 1.77 and 1.13 wt%, respectively, for HS(1.1)/Fe_3O_4@SiO_2, indicating that MPTES was successfully fixed on Fe_3O_4@SiO_2. The Si/Fe ratio and average diameter of the particles (D_{SEM}, Table 1) were slightly increased by the modification with MPTES, supporting the suggestion that MPTES was fixed on the surface of Fe_3O_4@SiO_2.

HS(1.1)/Fe_3O_4@SiO_2 gave five absorption bands, at 2808, 2867, 2896, 2937, and 2953 cm^{-1} assignable to C-H stretching of -CH_3 and -CH_2-. If MPTES was ideally fixed with three Si-O-Si bonds on Fe_3O_4@SiO_2, only two C-H stretching bands would have been observed because of the presence of only -CH_2- in Si-$(CH_2)_3$-SH. However, five absorption bands were in fact present in that region, suggesting the presence of Si-

OCH_2CH_3 in addition to Si-$(CH_2)_3$-SH. This will be discussed in detail later. No IR band assignable to SH stretching, which would be observed at around 2550-2650 cm^{-1}, was detected for HS(1.1)/Fe_3O_4@SiO_2. Neat propyl mercaptan gives only a very weak IR band due to SH stretching [29]. In addition, the concentration of SH on HS(1.1)/Fe_3O_4@SiO_2 was low due to the surface modification. Those were the reason for the absence of the band due to SH stretching for HS(1.1)/Fe_3O_4@SiO_2.

Surface density of SH over HS(1.1)/Fe_3O_4@SiO_2 was estimated from the sulfur content (1.13 wt%) and surface area (190 $m^2\ g^{-1}$) using Equation 1.

$$\text{Surface density of SH } (nm^{-2}) = \frac{\dfrac{\text{Sulfur content (wt\%)}/100}{\text{Atomic weight of sulfur}} \times \text{Avogadro's number}}{\text{Surface area } (m^2\ g^{-1}) \times 10^{18}\ (nm^2\ m^{-2})} \quad (1)$$

The calculated SH density was 1.1 nm^{-2}. If MPTES was fixed with three Si-O-Si bonds, the atomic ratio of C/S would be 3. However, the actual C/S atomic ratio for HS(1.1)/Fe_3O_4@SiO_2 measured by the elemental analysis was 4.2 (Table 1), suggesting that some ethoxy groups were remaining, as supported by the IR spectra. In other words, a part of MPTES was fixed on the surface with two or less Si-O-Si bonds. Here, assuming

that MPTES is fixed on the surface with three or two Si-O-Si bonds, we can estimate the fraction of MPTES fixed with two Si-O-Si bonds (α) using Equation 2:

$$\text{C/S atomic ratio} = 3\times(1-\alpha) + 5\alpha \quad (2)$$

where 3 and 5 are the numbers of carbon atoms contained in the moiety fixed on the surface with three and two Si-O-Si bonds, respectively, for ($Si(C_3H_6SH)$ and $Si(C_3H_6SH)(OC_2H_5)$, respectively. From the actual measured C/S atomic ratio (= 4.2), α was calculated to be 0.6, meaning that 60% of MPTES was fixed with two Si-O-Si bonds (Scheme 1).

We prepared HS(*x*)/Fe_3O_4@SiO_2 with different doses of MPTES and examined the relationship between the MPTES dose and the surface density of SH fixed on Fe_3O_4@SiO_2 (Fig. 5). The surface density of SH was linearly increased with increases in the MPTES dose up to close to 0.3 mmol g^{-1}. The increase in the surface density of SH slowed down with more doses of MPTES and finally the surface density reached a constant value of around 1.5 nm^{-2}. The further increase in the surface density of SH by the addition of excess MPTES dose (3.0 mmol g^{-1}) was probably due to self-condensation of MPTES.

3.3. Transformation of the thiol group of HS/Fe_3O_4@SiO_2 to sulfonic acid

Before investigating the impact of the surface SH density on catalytic performance, we selected HS(x)/Fe_3O_4@SiO_2 with x = 0.47, 1.1, and 1.4 nm^{-2} as typical samples and used them for oxidation of SH into SO_3H. The oxidation of SH with HNO_3 did not change the size (D_{XRD}) and crystalline structure of the Fe_3O_4 core, average diameter of the particle (D_{SEM}), or thickness of SiO_2 shell (Figs. 1 and 2, and Table 1). After the oxidation, the absorption band due to SH stretching at 2808 cm^{-1} disappeared and instead two absorption bands due to SO_3H appeared at 1578 and 1601 cm^{-1} for HSO_3(1.1)/Fe_3O_4@SiO_2 (Fig. 4(c)). In contrast to the sample before oxidation, only two bands were observed at 2896 and 2953 cm^{-1} in the CH stretching region. The disappearance of three bands (2808, 2867, and 2937 cm^{-1}) due to CH stretching suggested elimination of Si-OCH_2CH_3 from the sample during the oxidation. In addition, the broad band at 3230 cm^{-1} due to highly hydrogen-bonded OH stretching disappeared in the oxidation with HNO_3, which was probably due to condensation between residual silanols. However, Si-O-Si bonds formed by the condensation were not very strong and were

available for further modification with organosilanes, as described in section 3.4.

For HS(*x*)/Fe_3O_4@SiO_2, the sulfur content changed little as a result of oxidation (Table 1), indicating that oxidative decomposition and elimination of the mercaptopropyl group from HS(*x*)/Fe_3O_4@SiO_2 did not occur during the oxidation. However, carbon content was decreased by the oxidation with HNO_3 and the C/S atomic ratio became around 3 for every HSO_3(*x*)/Fe_3O_4@SiO_2. The decrease in the C/S atomic ratio by the oxidation of SH supports the deduction that the unreacted ethoxy groups left on HS(*x*)/Fe_3O_4@SiO_2 were eliminated by hydrolysis with the help of HNO_3.

Even after the oxidation, no peak due to Fe 2p was observed on the XPS spectrum for HSO_3(1.1)/Fe_3O_4@SiO_2 (Fig. 3(d)), indicating that the SiO_2 shell was stable during the oxidation process. The acid amounts of HSO_3(0.47)/Fe_3O_4@SiO_2, HSO_3(1.1)/Fe_3O_4@SiO_2, and HSO_3(1.4)/Fe_3O_4@SiO_2 estimation by the titration were 0.19, 0.40, and 0.56 mmol g^{-1}, respectively (Table 1), which were a little larger than the amounts of sulfur for each sample, being 0.21, 0.31, and 0.45 mmol g^{-1}, respectively. Since the measurements of acid amount for the samples before the oxidation indicated that those had certain amounts of acid sites (Table 1) despite without any sulfonic acid,

the method applied in this study counted silanol groups on $Fe_3O_4@SiO_2$ as acids. Thus, the acid amounts of $HSO_3(x)/Fe_3O_4@SiO_2$ were overestimated a little.

The catalytic performances of $HSO_3(0.47)/Fe_3O_4@SiO_2$, $HSO_3(1.1)/Fe_3O_4@SiO_2$, and $HSO_3(1.4)/Fe_3O_4@SiO_2$ were evaluated for hydrolysis of ethyl acetate in excess water (Fig. 6). All the catalysts promoted the reaction and the conversions were increased over the reaction time. Among the catalysts, $HSO_3(1.4)/Fe_3O_4@SiO_2$ showed the highest activity for the reaction. Fig. 5 indicates, however, that the surface density of SH reached a constant value for $HS(1.4)/Fe_3O_4@SiO_2$, and thus it might contain few silanol groups for further modification with triethoxy(ethyl)silane, triethoxy(octyl)silane and triethoxy(phenyl)silane. Hence, we concluded that $HSO_3(1.4)/Fe_3O_4@SiO_2$ was unsuited for further modification and thus selected $HSO_3(1.1)/Fe_3O_4@SiO_2$.

3.4. Further modification of $HSO_3(1.1)/Fe_3O_4@SiO_2$ with organic silanes and influence of the modification on the catalytic performance

Modifications of $HSO_3(1.1)/Fe_3O_4@SiO_2$ with triethoxy(ethyl)silane, triethoxy(octyl)silane, and triethoxy(phenyl)silane brought about an increase in the

carbon content (Table 1). The CH stretching on the IR spectrum for the sample modified with triethoxy(octyl)silane became strong, while the strength of IR bands due to SO_3H was unchanged (Fig. 4(d)). Those modifications did not change sulfur content or acid amounts. Using Equation 3, surface density of the modified *R* (= ethyl, octyl, or phenyl group) was calculated for the contents of carbon and sulfur, and surface area.

$$\text{Surface density of } R\ (\text{nm}^{-2}) = \frac{\text{Carbon content (wt\%)}/100 - \dfrac{\text{Sulfur content (wt\%)}/100}{\text{Atomic weight of sulfur}} \times (3 \times \text{Atomic weight of carbon})}{\text{Number of carbon atoms in } R \times \text{Atomic weight of carbon}} \times \frac{\text{Avogadro's number}}{\text{Surface area } (\text{m}^2\,\text{g}^{-1}) \times 10^{18}\ (\text{nm}^2\,\text{m}^{-2})} \quad (3)$$

Although there was some difference depending on the kind of organic silane, the surface density of *R* was about 2 nm^{-2}, meaning that *R* and SO_3H were present on the surface with a 2 to 1 ratio (Table 1). In Fig. 7, a schematic image of the surface is illustrated, in which Si-$(CH_2)_3$-SO_3H and Si-*R* are assumed to be regularly arranged. A propyl sulfonic silane (-$(CH_2)_3$-SO_3H) is surrounded by four Si-*R* on average and the average distance between Si-$(CH_2)_3$-SO_3H and Si-*R* is estimated to be 0.5 nm. Because van der Waals' radius of $-CH_2-$ is about 0.2 nm, Si-$(CH_2)_3$-SO_3H and Si-*R* are densely packed over the surface.

Fig. 8 shows adsorption isotherms of water vapor taken at 298 K for $HSO_3(1.1)/Fe_3O_4@SiO_2$, $Et/HSO_3(1.1)/Fe_3O_4@SiO_2$, $Oc/HSO_3(1.1)/Fe_3O_4@SiO_2$, and $Ph/HSO_3(1.1)/Fe_3O_4@SiO_2$. In the case of the unmodified $HSO_3(1.1)/Fe_3O_4@SiO_2$, the adsorption amount of water vapor steeply increased in the low-pressure region ($P/P_0 <$ 0.02), indicating that the surface was hydrophilic. In contrast, the adsorption amounts of water vapor in the low-pressure region were considerably suppressed for the organosilane-modified samples. The lower adsorption of water vapor indicated that the surface became hydrophobic as a result of the modifications with organosilane, and especially with octylsilane. As was mentioned above, there was little difference in the surface density of Si-*R* (about 2.0 nm^{-2}), regardless of the kind of organosilane. In addition, little Si-OH was remaining over the modified samples. Thus, the kind of *R* had a strong impact on the adsorption properties for water vapor. Apparently, the molecular length of the ethyl group is shorter than that of propylsulfonic acid. Thus, sulfonic acid on $Et/HSO_3(1.1)/Fe_3O_4@SiO_2$ was not surrounded by ethyl groups in the bare state (Fig. 9A). At such acidic sites, water molecules would be able to approach easily. Molecular length of the phenyl group is comparable to, but somewhat shorter than, that of propyl

sulfonic acid (Fig. 9C). Thus, it is reasonable that the sulfonic acid group still protrudes from the surface created by the phenyl groups and such acid sites attract water molecules. In contrast, the edges of the octyl group can surround the sulfonic acid over Oc/HSO_3(1.1)/Fe_3O_4@SiO_2, because the molecular length of the octyl group is longer than that of propylsulfonic acid (Fig. 9B). The hydrophobic environment around the sulfonic acid group caused by octyl groups could weaken the power of sulfonic acid to attract water molecules, as observed in the reduction of the amount of water molecules on the adsorption isotherm.

The catalytic performances of HSO_3(1.1)/Fe_3O_4@SiO_2, Et/HSO_3(1.1)/Fe_3O_4@SiO_2, Oc/HSO_3(1.1)/Fe_3O_4@SiO_2, and Ph/HSO_3(1.1)/Fe_3O_4@SiO_2 for hydrolysis of ethyl acetate in water are compared in Fig. 10. All the organosilane-modified catalysts exhibited catalytic activities higher than that of the unmodified HSO_3(1.1)/Fe_3O_4@SiO_2. Among them, Oc/HSO_3(1.1)/Fe_3O_4@SiO_2 showed the highest activity. The conversion at 6 h for Oc/HSO_3(1.1)/Fe_3O_4@SiO_2 was about twice that of HSO_3(1.1)/Fe_3O_4@SiO_2. The order of the catalytic performances correlated well with that of the hydrophobicity evaluated by the adsorption isotherm of water vapor. The catalyst with the highest

hydrophobic surface gave the highest catalytic activity in water. It is proposed that enhancement of hydrophobicity over the surface or around the active site is an effective way to reduce poisoning of the active site with water, leading to the development of highly active solid acid catalysts for use in water [5]. In our catalysts, two factors were achieved by the further modification of octylsilane by the controlled amount: (i) significant enhancement of hydrophobicity over the surface caused by the capping of silanol and (ii) creating a hydrophobic environment around acid sites. The sulfonic acid in such hydrophobic environments was not subjected to severe poisoning by water and consequently showed high catalytic activity for acid catalyzation in water.

Table 2 compares the catalytic performance of $Oc/HSO_3(1.1)/Fe_3O_4@SiO_2$ for hydrolysis of ethyl acetate in water with various acid catalysts reported in the literature [25, 30] under the same reaction conditions as applied in the present study. As Table 2 clearly demonstrates, the activity of $Oc/HSO_3(1.1)/Fe_3O_4@SiO_2$ was higher than $H_3PW_{12}O_{40}$, its Cs salt, and the one anchored on the hydrophobic surface ($H_3PW_{12}O_{40}/C_8$-AP-SBA), if compared per catalyst weight. It should be noted that $Oc/HSO_3(1.1)/Fe_3O_4@SiO_2$ had activity comparable to them if compared per acid sites,

though the acid strength of sulfonic acid was much weaker than that of $H_3PW_{12}O_{40}$, which is known as a super acid [31], being 115 and 200 kJ mol^{-1}, respectively [22, 32], evaluated by ammonia adsorption calorimetry. The highly hydrophobic environment around the acid sites over $Oc/HSO_3(1.1)/Fe_3O_4@SiO_2$ could suppress the poisoning of the acid site with water, leading to high catalytic activity in water.

In addition to the improvement in catalytic activity, modification with octylsilane enhanced the stability of the catalyst for repeated uses in water. Fig. 11 shows the results of the repeated uses of the unmodified and octylsilane-modified catalysts in hydrolysis of ethyl acetate. Both catalysts were magnetically collected within 1 min (upper photos in Fig. 11). In the case of $HSO_3(1.1)/Fe_3O_4@SiO_2$, the conversion was gradually decreased over repeated uses. The catalytic activity after four-times reuse was decreased by 20% compared to that of the fresh catalyst. On the other hand, $Oc/HSO_3(1.1)/Fe_3O_4@SiO_2$ was very stable for repeated use and degradation in catalytic performance over repeated use was small. Over the hydrophobic surface created by octyl modification, it is hard for water molecules to approach the silica surface in water, which suppresses elimination of propylsulfonic acid by hydrolysis of the Si-O-Si bond connecting to the surface, leading

to high stability in repeated use in water.

Conclusions

We developed octyl and propylsulfonic acid co-fixed Fe_3O_4@SiO_2 as a magnetically separable and highly active solid acid catalyst for hydrolysis of ethyl acetate in water. In the optimized catalyst, the surface density of propylsulfonic acid groups was about 1 nm^{-2}, and they were surrounded by four octyl groups with a distance of 0.5 nm from the propylsulfonic acid on average. The catalyst was easily separated from the reaction solution by an external magnetic field. The catalyst showed activity about twice as high as that of the catalyst without octyl modification. Modification of propylsulfonic acid-fixed Fe_3O_4@SiO_2 with ethyl and phenyl groups enhanced the catalytic performance, but the enhancement in the activity was less than for octyl group modification. In addition to the higher catalytic activity, the modification of propylsulfonic acid-fixed Fe_3O_4@SiO_2 with octyl groups provided high stability for repeated use of the catalyst in hydrolysis of ethyl acetate in water and there was little decrease in activity over four reuses. High hydrophobicity over the surface and around the acid sites (SO_3H) by the octyl group was

responsible for the high catalytic activity and high stability in water.

Acknowledgements

The authors gratefully acknowledge the Ministry of Research, Technology and Higher Education, Indonesia for financial support through its World Class Professor Program in preparation of this publication under contract number 123.19/D2.3/KP/2018. One of the authors (Mrs. Ani Qomariyah) would also like to thank the Japanese Government's Japanese Student Service Organization (JASSO) for financial support in conducting the research.

References

[1] M.M. Kirchhoff, 2005, Promoting Sustainability through Green Chemistry, Conservation and Recycling, 44, 237-243.

[2] P.T. Anastas, M.M. Kirchhoff, T.C. Williamson, Appl. Catal. A 221 (2001) 3-13.

[3] P. Gupta, S. Paul, Catal. Today 236 (2014) 153-170.

[4] R.A. Sheldon, S.S. Downing, Appl. Catal. A 189 (1999) 163-183.

[5] T. Okuhara, Chem. Rev. 102 (2002) 3641-3666.

[6] R.D. Badley, W.T. Ford, J. Org. Chem. 54 (1989) 5437-5443.

[7] C.T. Kresge, M.E. Leonowicz, W.J. Royh, J.C. Vartluti, J.S. Beck, Nature 359 (1992) 710-712.

[8] Y. Yonagisawa, T. Shimizu, K. Kuroda, C. Kato, Bull. Chem. Soc. Jpn. 63 (1990) 988-992.

[9] G.M. Ziarania, N. Lashgarib, A. Badieib, J. Mol. Catal. A 397 (2015) 166–191.

[10] D.P. Sawant, A. Vinu, S.P. Mirajkar, F. Lefebvre, K. Ariga, S. Anandan, T. Mori, C. Nishimura, S.B. Halligudi, J. Mol. Catal. A 271 (2007) 46-56.

[11] S. Sulastri, N. Nuryono, I. Kartini, E. S. Kunarti, Indones. J. Chem. 11, (2011) 273-

278.

[12] D. Dufaud, M.E. Davis, J. Am. Chem. Soc. 125 (2003) 9403-9413.

[13] W.M. Van Rhijn, D.E. De Vos, B.F. Sels, W.D. Bossaert, P.A. Jabobs, Chem. Commun. (1998) 317-318.

[14] J.A. Melero, R. van Grieken, G. Morales, Chem. Rev., 106 (2006) 3790-3812.

[15] A. Corma, H. Garcia, Adv. Synth. Catal. 348 (2006) 1391-1412.

[16] M.A. Harmer, Q. Sun, M.J. Michalczyk, Z. Yang, Chem. Commun. (1997) 1803.

[17] M. Alvaro, A. Corma, D. Das, V. Fornésa H. García, Chem. Commun. (2004) 956-957.

[18] M. Alvaro, A. Corma, D. Das, V. Fornés, H. García, J. Catal. 231 (2005) 48-55.

[19] D.J. Macquarrie, S.J. Tavener, M.A. Harmer, Chem. Commun. (2005) 2363-2364.

[20] Z. Yang, W. Qi, R. Huang, J. Fang, R. Su, A. He, Chem. Eng. J. 296 (2016) 209-216.

[21] A. Cubo, J. Iglesias, G. Morales, J.A. Melero, J. Moreno, R. Sánchez-Vázquez, Appl. Catal. A 531 (2017) 151-160.

[22] J. Dacquin, H.E. Cross, D.R. Brown, T. Duren, J.J. Williams, A. Lee, K. Wilson,

Green Chem. 12 (2010) 1383-1391.

[23] J.C. Manayil, V.C. dos Santos, F.C. Jentoft, M.G. Mesa, A.F. Lee, K. Wilson, ChemCatChem 9 (2017) 2231-2238.

[24] I.K. Mbaraka, B.H. Shanks, J. Catal. 229 (2005) 365-373.

[25] K. Inumaru, T. Ishihara, Y. Kamiya, T. Okuhara, S. Yamanaka, Angew. Chem. Int. Ed. 46 (2007) 7625-7628.

[26] H. Hattori, Y. Ono, Solid Acid Catalysis from Fundamental to Applications, Pan Stanford Publishing, USA, 2015, p.25-47.

[27] N. Nuryono, N.M. Rosiati, B. Rusdiarso, S.C.W. Sakti, S. Tanaka, SpringerPlus, 3 (2014) 515-526.

[28] D.Yang, J. Hu, S. Fu, J. Phys. Chem. C 113 (2009) 7646-7651.

[29] L.J. Bellamy, The Infra-red Spectra of Complex Molecules, Chapman and Hall, London, (1975) p.395.

[30] M. Kimura, T. Nakato, T. Okuhara, Appl. Catal A 165 (1997) 227-240.

[31] T. Okuhara, N. Mizuno, M. Misono, Adv. Catal. 41 (1996) 113-252.

[32] F. Lefebvre, F.X. Liu-Cai, A. Auroux, J. Mater. Chem. 4 (1994) 125-131.

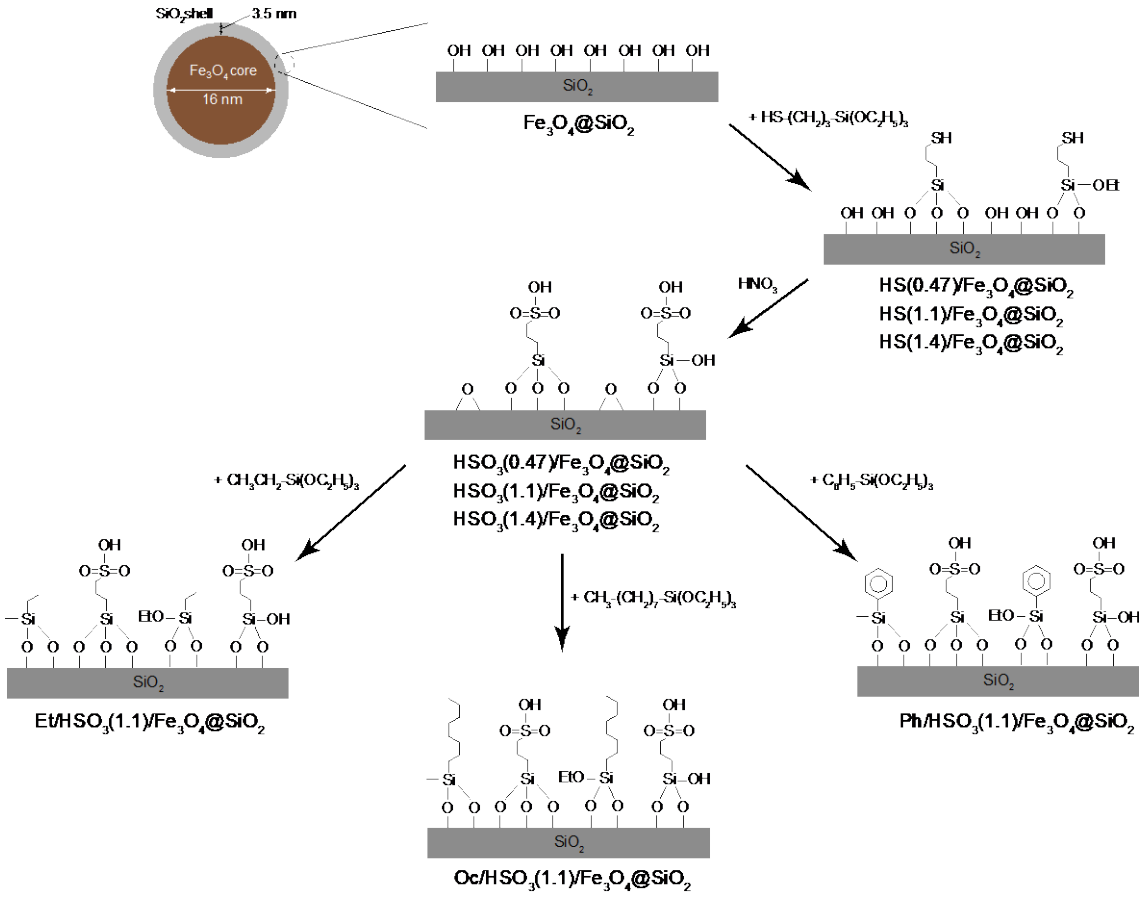

Scheme 1 The samples prepared in this study.

Table 1 Physical and chemical properties of the prepared samples.

	Si/Fe	D_{XRD}[a]	D_{SEM}[b]	Surface area	Elemental analysis /wt%		Surface density[c] /nm^{-2}		Acid amount
		/nm	/nm	/m^2 g^{-1}	C	S	SH (or SO_3H)	R[d]	/mmol g^{-1}
Fe_3O_4	---	16.8	12.5	78	---	---	---	---	---
Fe_3O_4@SiO_2	5.9	16.4	23.0	196	---	---	---	---	---
HS(0.47)/Fe_3O_4@SiO_2	6.4	---	---	191	1.04	0.48	0.47	---	0.08
HS(1.1)/Fe_3O_4@SiO_2	6.7	17.0	21.5	190	1.77	1.13	1.1	---	0.20
HS(1.4)/Fe_3O_4@SiO_2	7.0	---	---	185	2.10	1.40	1.4	---	0.09
HSO_3(0.47)/Fe_3O_4@SiO_2	---	---	---	229	1.06	0.67 (0.21)[e]	0.55	---	0.19
HSO_3(1.1)/Fe_3O_4@SiO_2	6.9	16.6	24.0	225	1.37	0.99 (0.31)[e]	0.83	---	0.40
HSO_3(1.4)/Fe_3O_4@SiO_2	---	---	---	215	1.79	1.43 (0.45)[e]	1.2	---	0.56
Et/HSO_3(1.1)/Fe_3O_4@SiO_2	---	---	---	208	3.65	1.01	0.91	2.3	0.45
Oc/HSO_3(1.1)/Fe_3O_4@SiO_2	---	---	---	193	7.98	1.04	1.0	2.0	0.46
Ph/HSO_3(1.1)/Fe_3O_4@SiO_2	---	---	---	153	5.84	1.00	1.2	2.3	0.48

[a]Crystallite size estimated by using Scherer's equation with line width of the diffraction line due to (311) of Fe_3O_4 on powder XRD patterns.

[b]Average diameter of the particles estimated from SEM images.

[c]Estimated from elemental analysis and surface area by using eqs. 1 and 3.

[d]*R* = ethyl, octyl, or phenyl group.

[e]Sulfur contents expressed with mmol g^{-1}.

Table 2 Comparison of acidity and activity for hydrolysis of ethyl acetate in water over Oc/$HOSO_2$/Fe_3O_4@SiO_2 with the reported data.

Catalyst	State of catalysts[a]	Acidity of catalyst /mmol g^{-1}	Catalytic activity		Reference
			per catalyst weight /μmol min^{-1} g_{cat}^{-1}	per acidic protons /mmol min^{-1} mol_{acid}^{-1}	
H_2SO_4	liquid	19.8	992	46	[30]
HY zeolite	solid	2.6	0	0	[30]
γ-Al_2O_3	solid	0.47	0	0	[30]
H-ZSM-5 zeolite	solid	0.39	27.6	70	[30]
SO_4^{2-}/ZrO_2	solid	0.35	25.5	127	[30]
Nafion-H resin	solid	0.8	162	202	[30]
$Cs_{2.5}H_{0.5}PW_{12}O_{40}$	solid	0.15	30.1	200	[30]
$H_3PW_{12}O_{40}$	liquid	1.0	78.7	78	[25]
$H_3PW_{12}O_{40}$/C_8-AP-SBA[b]	solid	0.091	25.1	275	[25]
Oc/HSO_3(1.1)/Fe_3O_4@SiO_2	solid	0.52	107	205	This work

[a]Liquid, homogeneous catalysis and solid, heterogeneous catalysis.

[b]$H_3PW_{12}O_{40}$ supported on octyl and 3-aminopropyl groups co-fixed on SBA-15.

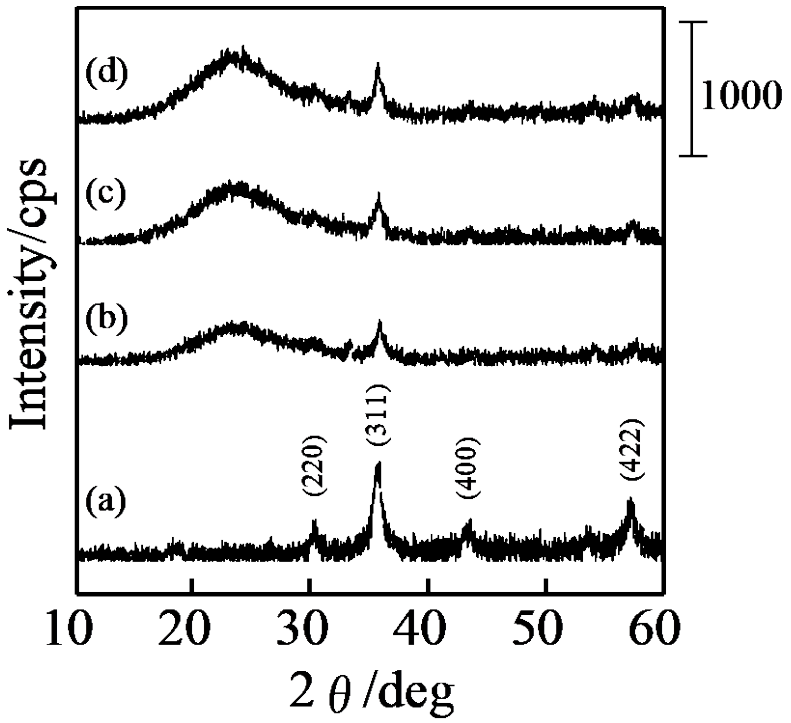

Fig. 1 XRD patterns of (a) Fe_3O_4, (b) Fe_3O_4@SiO_2, (c) HS(1.1)/Fe_3O_4@SiO_2, and (d) HSO_3(1.1)/Fe_3O_4@SiO_2.

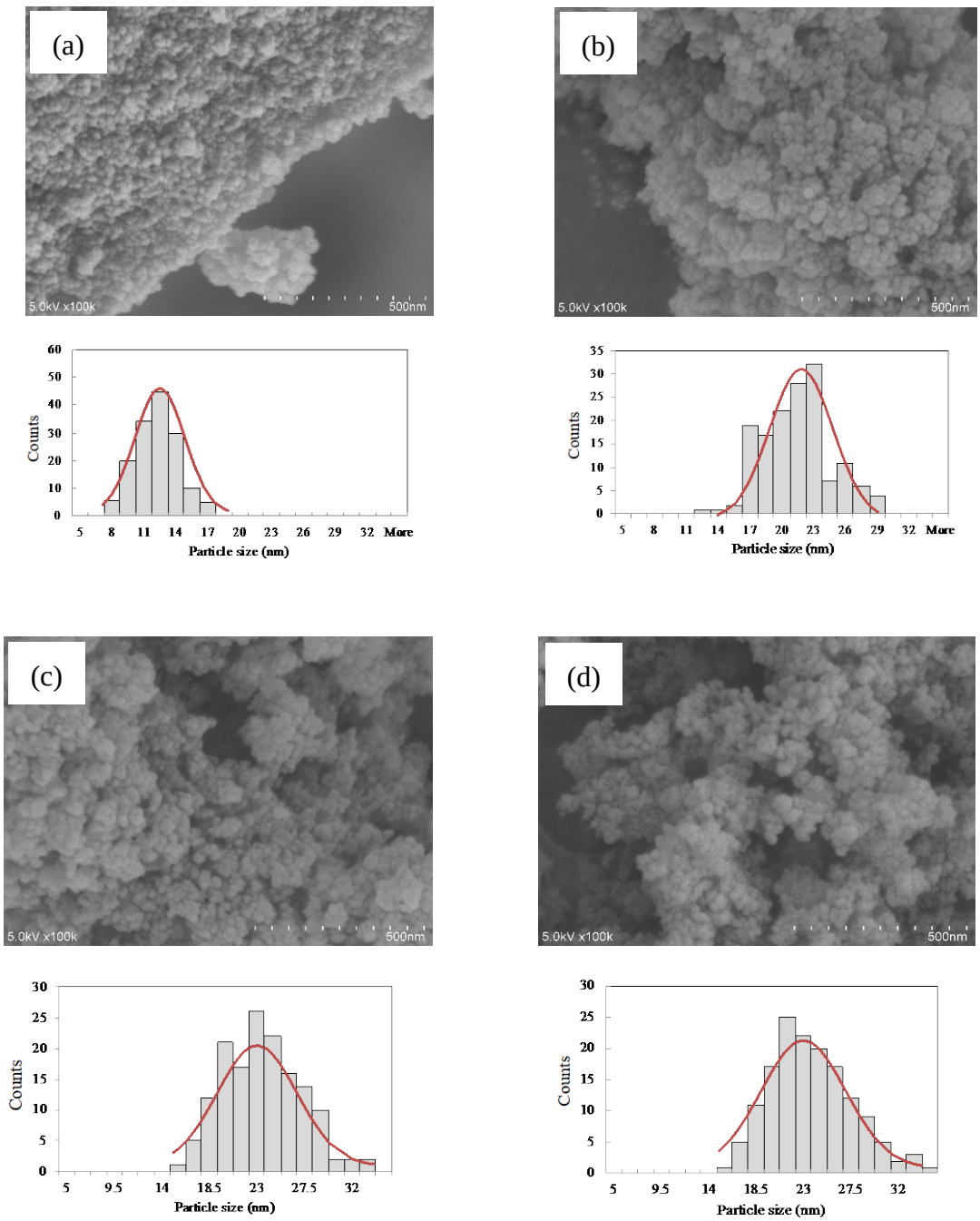

Fig. 2 SEM images and particle size distributions of (a) Fe_3O_4, (b) $Fe_3O_4@SiO_2$, (c) $HS(1.1)/Fe_3O_4@SiO_2$, and (d) $HSO_3(1.1)/Fe_3O_4@SiO_2$.

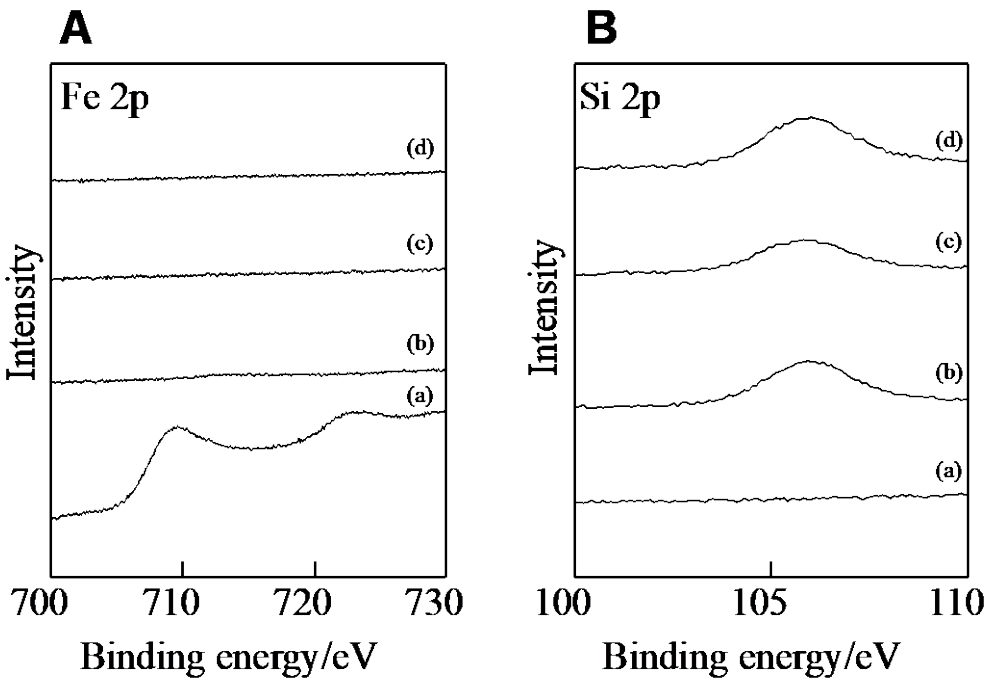

Fig. 3 XPS spectra of (A) Fe 2p and (B) Si 2p for (a) Fe_3O_4, (b) $Fe_3O_4@SiO_2$, (c) $HS(1.1)/Fe_3O_4@SiO_2$, and (d) $HSO_3(1.1)/Fe_3O_4@SiO_2$.

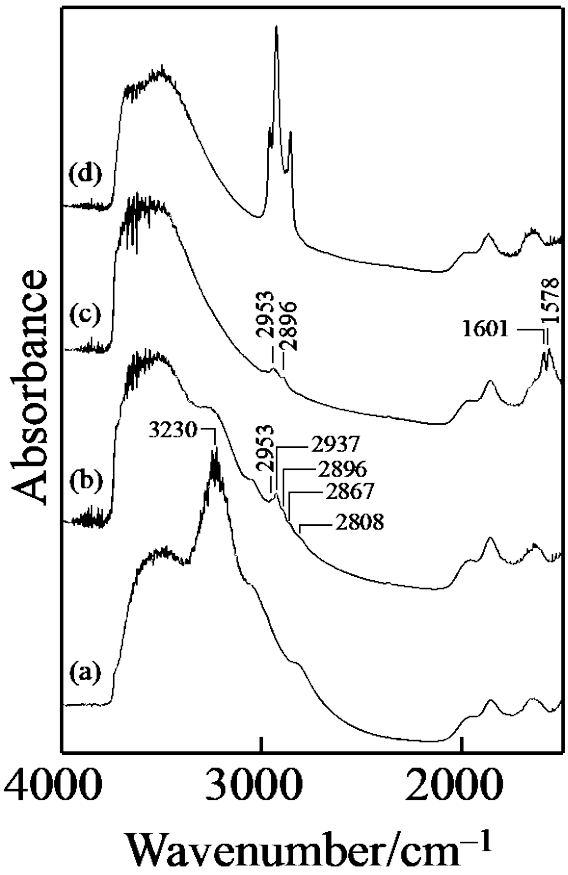

Fig. 4 IR spectra of (a) Fe_3O_4@SiO_2, (b) HS(1.1)/Fe_3O_4@SiO_2, and (c) HSO_3(1.1)/Fe_3O_4@SiO_2 and (d) Oc/HSO_3(1.1)/Fe_3O_4@SiO_2. The spectra were taken with self-supporting disks.

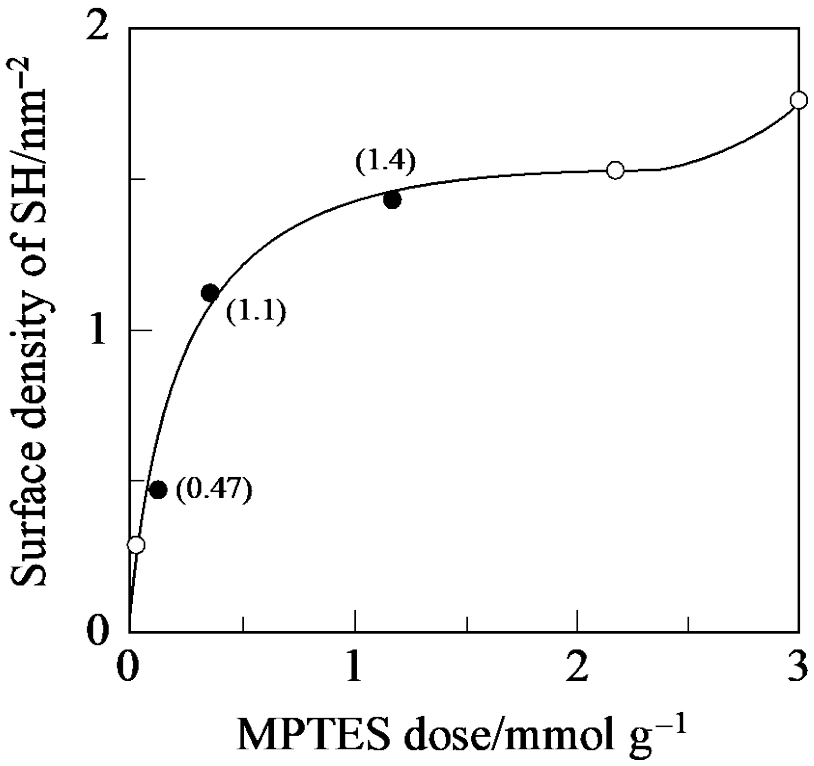

Fig. 5 Surface density of SH fixed on Fe_3O_4@SiO_2 plotted as a function of dose of 3-mercaptotriethoxyproplsilane (MPTES) per unit weight of Fe_3O_4@SiO_2. Surface density of SH was calculated from sulfur content and surface area by using eq. 1. The samples represented with a filled circle are those applied for further treatment and provided for the catalytic reaction shown in Fig. 6.

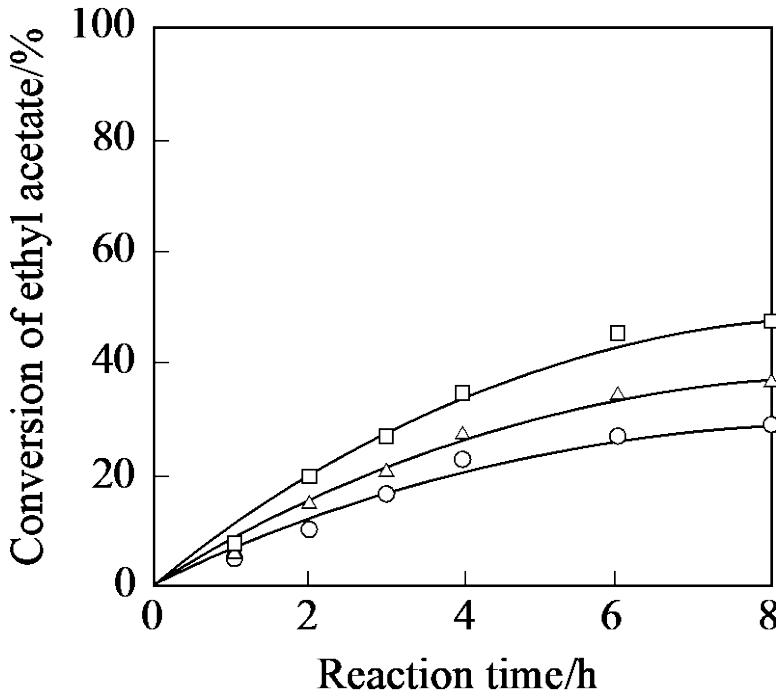

Fig. 6 Catalytic performance for hydrolysis of ethyl acetate in water over (○) $HSO_3(0.47)/Fe_3O_4@SiO_2$, (△) $HSO_3(1.1)/Fe_3O_4@SiO_2$, and (□) $HSO_3(1.4)/Fe_3O_4@SiO_2$.

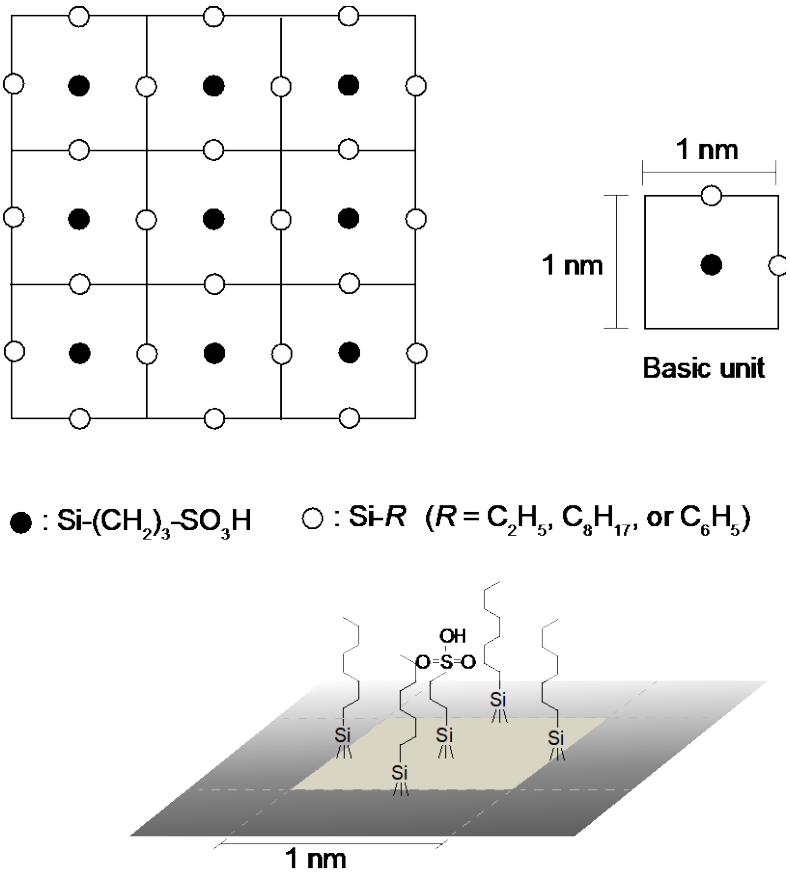

Fig. 7 A schematic image of the surface for *R*/HSO_3(1.1)/Fe_3O_4@SiO_2. *R* = ethyl, octyl, or phenyl.

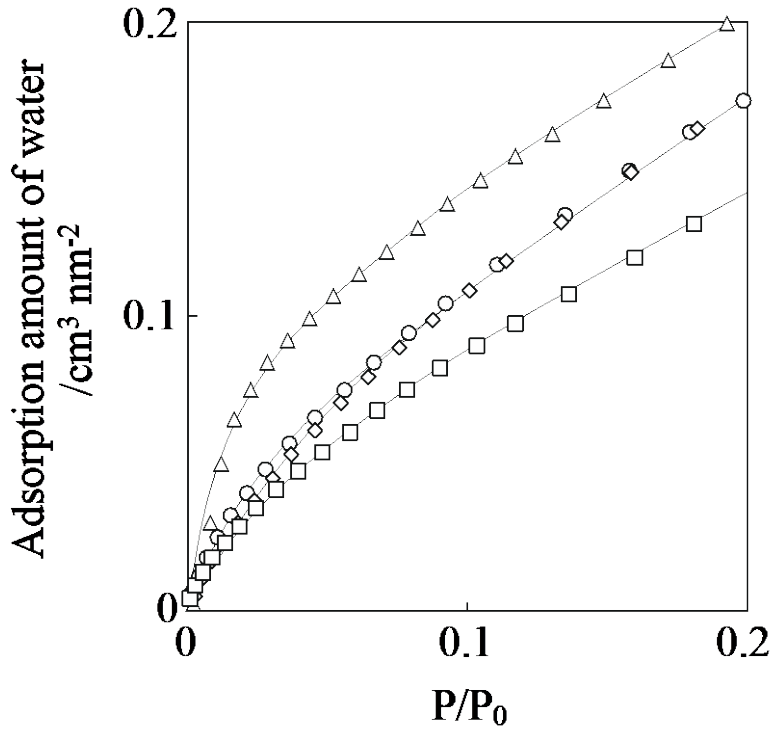

Fig. 8 Adsorption isotherms of water vapor at 298 K for (△) $HSO_3(1.1)/Fe_3O_4@SiO_2$, (○) $Et/HSO_3(1.1)/Fe_3O_4@SiO_2$, (□) $Oc/HSO_3(1.1)/Fe_3O_4@SiO_2$ and (◇) $Ph/HSO_3(1.1)/Fe_3O_4@SiO_2$.

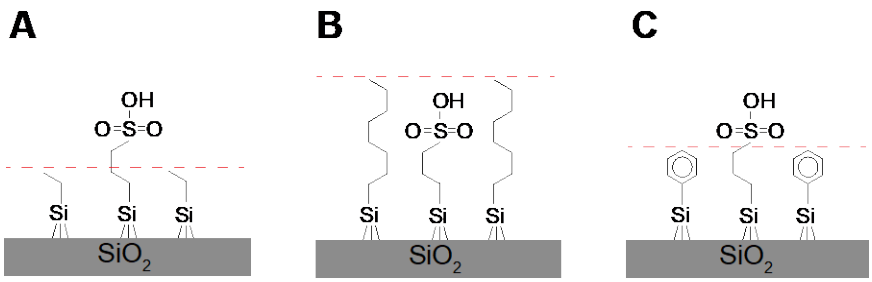

Fig. 9 Comparison of molecular length of propylsulfonic acid with those of ethyl, octyl, and phenyl groups. (A) Et/HSO_3(1.1)/Fe_3O_4@SiO_2, (B) Oc/HSO_3(1.1)/Fe_3O_4@SiO_2 and (C) Ph/HSO_3(1.1)/Fe_3O_4@SiO_2.

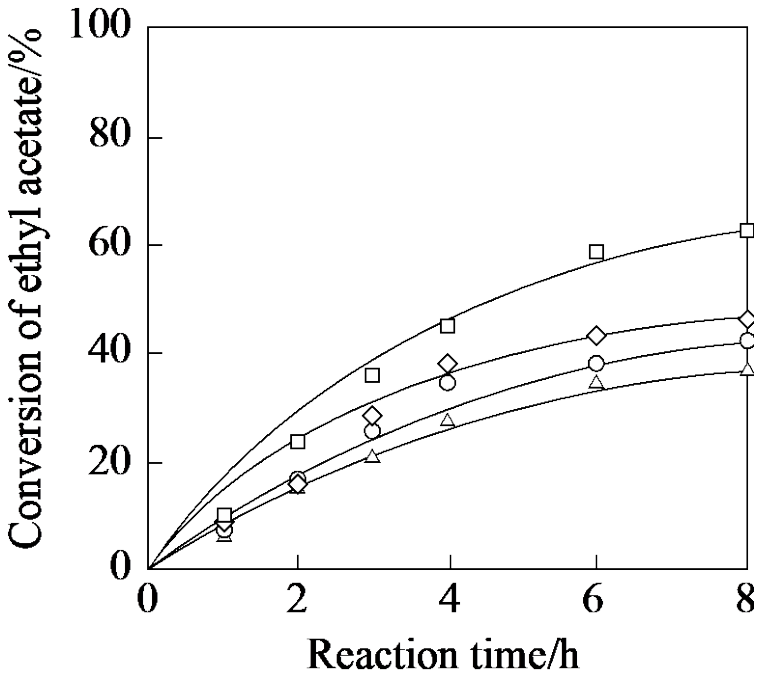

Fig. 10 Catalytic performance for hydrolysis of ethyl acetate in water over (△) $HSO_3(1.1)/Fe_3O_4@SiO_2$, (○) $Et/HSO_3(1.1)/Fe_3O_4@SiO_2$, (□) $Oc/HSO_3(1.1)/Fe_3O_4@SiO_2$ and (◇) $Ph/HSO_3(1.1)/Fe_3O_4@SiO_2$.

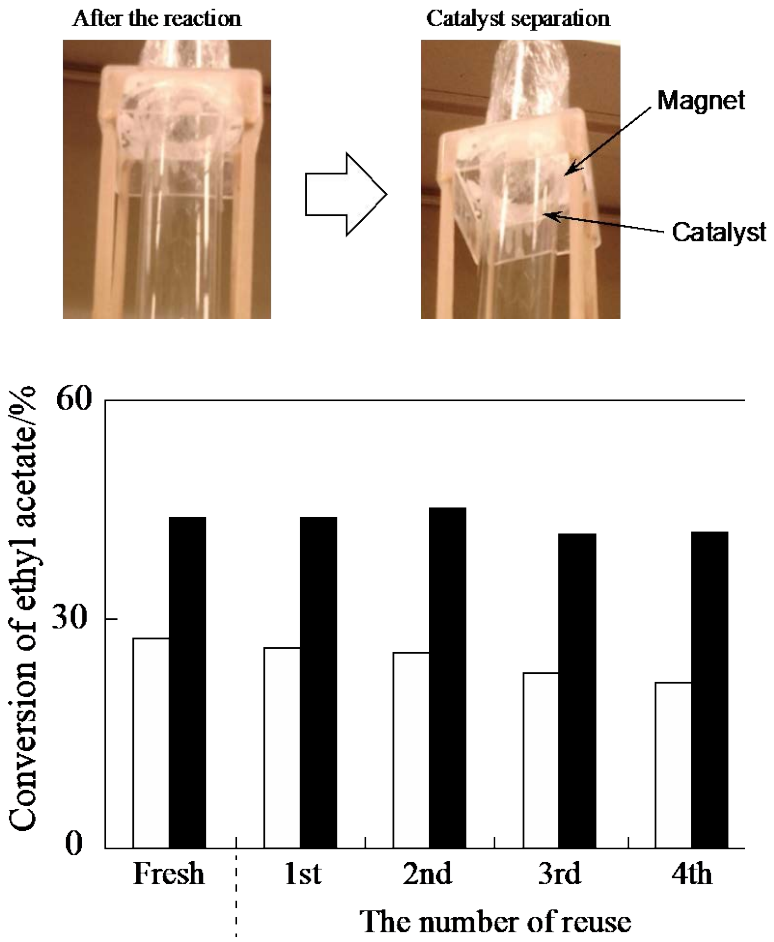

Fig. 11 Reusability tests of (■) $HSO_3(1.1)/Fe_3O_4@SiO_2$ and (□) $Oc/HSO_3(1.1)/Fe_3O_4@SiO_2$ for hydrolysis of ethyl acetate in water. Upper photos are the look of catalyst separation with a magnet.